

Quality assessment of dental treatments using *en-face* optical coherence tomography

Cosmin Sinescu
Meda Lavinia Negrutiu
Carmen Todea
Cosmin Balabuc
Laura Filip
Roxana Rominu

Victor Babes University of Medicine and Pharmacy
of Timisoara
School of Dentistry
Bd. Revolutiei din 1989 Nr. 9
300070, Timisoara, Romania

Adrian Bradu
Michael Hughes
Adrian Gh. Podoleanu

University of Kent
School of Physical Sciences
Applied Optics Group
Canterbury, CT2 7NH
United Kingdom

Abstract. The present study evaluates the potential of *en-face* optical coherence tomography (OCT) as a possible noninvasive high resolution method for supplying necessary information on the material defects of dental prostheses and microleakage at prosthetic interfaces. Teeth are also imaged after several treatment methods to assess material defects and microleakage at the tooth-filling interface, and the presence or absence of apical microleakage, as well as to evaluate the quality of bracket bonding on dental hard tissue. C-scan and B-scan OCT images as well as confocal images are acquired from a large range of samples. Gaps between the dental interfaces and material defects are clearly exposed. © 2008 Society of Photo-Optical Instrumentation Engineers. [DOI: 10.1117/1.2992593]

Keywords: optical coherence tomography; confocal microscopy; dental treatment; dental hard tissues; dental prostheses.

Paper 08132R received Apr. 21, 2008; revised manuscript received Aug. 13, 2008; accepted for publication Aug. 14, 2008; published online Oct. 6, 2008.

1 Introduction

Several methods are utilized in the practice of dental prostheses investigation.¹ The metallographic method² consists of successive removal of different thickness layers from the prosthesis body, followed by microscope investigation of the material defects found. Another method that is currently evolving is the method of penetrating liquids,³ which discloses surface defects only. These methods lead to sample destruction.⁴ Nondestructive methods are radiology, CT, and NMR; however, the first two are invasive for the patient and are limited to the detection of metal cast defects.⁵ Such methods exhibit poor resolution, and none have been developed to provide 3-D views of the defects within the material structure.

Good quality assessment requires noninvasive identification of much smaller defects than the size and resolution achievable by any of the methods in use today. It is desirable to be able to image individual defects and evaluate their overall distribution within the prosthesis. Once a defect is localized and characterized, the prosthesis is subject to further tests to evaluate its reliability under masticatory forces.

Several studies have demonstrated the potential of optical coherence tomography (OCT) to image, both hard and soft oral tissues⁶ at high resolution. OCT images provide microstructural details that cannot be obtained with any other imaging modalities. Periodontal tissue contour, sulcular depth, and connective tissue attachment⁷ can be identified in OCT images. The internal aspect and marginal adaptation of porcelain-fused-to-metal crowns and composite restorations can also be visualized.

An important goal in conservative dentistry is the evaluation of the microleakage in cavities filled with restorative materials. Presently, the methods used for assessing marginal microleakages are invasive and are performed *in vitro* only.^{8,9} The OCT potential for clinical evaluation of dental restoration¹⁰ has been demonstrated on interfaces between enamel and dental amalgam. Other studies have demonstrated that polarization-sensitive OCT is well suited for the imaging of demineralized and fluoride-enhanced remineralized artificial lesions,¹¹ as well as of interproximal and occlusal caries, early root caries, and for imaging decay under composite fillings,¹² composite sealants, and restorations.¹³

The success rate of root canal treatment and filling represents a challenge for the dentist. The incorrect filling of the root canal causes microleakage, which leads finally to the failure of endodontic therapy. There are several methods for evaluating the apical sealing of root canal sealers, such as bacterial penetration, fluid transport and clarification, penetration of radioisotopes, electrochemical methods, and gas chromatography.^{14,15} All these are either invasive, leading to sample destruction, or require expensive analytical infrastructure. Furthermore, they may lead to nonconclusive results. Therefore, OCT was proposed as a potential tool¹⁶ for *in-vivo* endodontic imaging.

All the OCT studies mentioned used A- or B-scan OCT techniques only. We use *en-face* OCT, which is based on transverse scanning.¹⁷ This allows C-scan imaging as well as an easy switch from C-scan to B-scan OCT. Several reports have demonstrated the utility of the *en-face* view in ophthalmology,¹⁸ and imaging of several pathologies has shown that the *en-face* view has allowed a quicker detection of retinal features, sometimes missed by longitudinal OCT.

Address all correspondence to: Meda Negrutiu, School of Dentistry, Victor Babes University of Medicine and Pharmacy of Timisoara, Bd. Revolutiei din 1989 Nr. 9, cod 300070, Timisoara, Romania. Tel: +40745166620; E-mail: meda_negrutiu@yahoo.com

In this work, *en-face* optical coherence tomography (OCT) is assessed as a possible noninvasive high resolution method in supplying information on the defect content of dental prostheses. A variety of prostheses have been imaged, either fixed or removable, and which are made of metal-ceramic, metal-polymer, all ceramic, and polymer.

The common methods currently used in the investigation of the quality of brackets bonding on tooth surfaces are based on the assessment of the shear bond strength.¹⁹ These methods are used for *in-vitro* experimental studies only and therefore there is still no *in-vivo* method for investigating the bracket-resin-tooth interfaces.

We have also investigated the potential of *en-face* OCT in evaluating the success of fixed orthodontic therapy. This depends, among other factors, on the bond strength of the bracket. OCT imaging presents good potential for *in-vivo* use; therefore, as a preliminary step before proceeding *in vivo*, we focused our attention mainly on the bracket-resin-tooth interface. We investigate further the marginal microleakage of composite resin fillings, the material defects inside the filling material, as well as the quality of the root canal filling.

The *en-face* view has also triggered development of dual OCT/fundus imaging.²⁰ Using the expertise acquired in combining OCT with confocal microscopy (CM), it becomes possible to investigate the utility of such dual imaging capability in dentistry. There may be instances where dual imaging, in the form of OCT/CM, proves better suited than an OCT investigation alone. Preliminary studies have indicated that such a dual display may provide useful information on the sample and may help the association of features seen in the high resolution image (OCT) with the bulk appearance of the "overall" view image, provided by a microscopy channel.²¹

In addition, due to the capability of *en-face* OCT to generate views in orthogonal planes (B- and C-scans) in real time, such an imaging method seems better suited to deliver tomography information. T-scan-based OCT has already been used to quantify the amount of mineral lost during the demineralization process²² of the enamel.

The purpose of this study is to investigate further the utility of *en-face* OCT in dentistry by evaluating the dental hard tissue, restorative materials, and their interfaces, as well as dental prostheses.

2 Material and Methods: Different Scanning Procedures

To obtain 3-D information about an object under investigation, any imaging system is equipped with three scanning means, one to scan the object in depth and two others to scan the object transversally. Depending on the order that these scanners are operated and on the scanning direction associated with the line displayed in the raster of the final image delivered, different possibilities exist.¹⁷

2.1 Longitudinal Optical Coherence Tomography (A-Scan-Based B-Scan)

B-scan images, analogous to ultrasound B-scans, are generated by collecting many reflectivity profiles in depth (A-scans) for different and adjacent transverse positions. The transverse scanner (operating along x or y) advances at a slower pace to build a B-scan image. The majority of reports

in the literature refer to this method of operation.^{6,7,10-13} In longitudinal OCT, the axial scanner is the fastest and its movement is synchronous with displaying the pixels along the line in the raster, while the lateral scanning determines the frame rate.

2.2 En-Face Optical Coherence Tomography (T-Scan-Based B-Scan)

In this case, the transverse scanner determines the fast lines in the image. We call each such image line a T-scan. This can be produced by controlling either the transverse scanner along the x coordinate, or along the y coordinate with the other two scanners fixed. This procedure has a net advantage in comparison with the A-scan-based B-scan procedure, as it allows production of OCT transverse (or 2-D *en-face*) images for a fixed reference path, images called C-scans.¹⁷ In this way, the system can be easily switched from B- to C-scan, a procedure incompatible with A-scan-based OCT imaging.

2.3 C-Scan

C-scans are made from many T-scans along either x or y , repeated for different values of the other transverse coordinate, y , x , respectively, in the transverse plane. The repetition of T-scans along the other transverse coordinate is performed at a slower rate than that of the T-scans, which determines the frame rate. In this way, a complete raster is generated. Different transversal slices are collected for different depths z , either by advancing the optical path difference in the OCT in steps after each complete transverse (xy) scan, or continuously at a much slower speed than the frame rate. Depth scanning is the slowest in this case.^{23,24}

2.4 Experimental Configuration

Two *en-face* OCT systems have been used. Both use similar pigtailed superluminescent diodes (SLD) emitting at 1300 nm and having spectral bandwidths of 65 nm, which determine an OCT longitudinal resolution of around 17.3 μm in tissue. The first OCT system performs OCT only, equipped with a low numerical aperture (NA) interface optics, which allows 1-cm lateral image size. The second system uses a higher NA interface optics with a maximum 1-mm image size. In addition, the second system is equipped with a confocal channel at 970 nm. The configuration of the second system, as shown in Fig. 1, uses two single mode directional couplers. Light from the SLD source is injected into the system via a first directional coupler, which splits the light toward the two arms of the interferometer, the probing and reference arms respectively. The probing beam is reflected by the dichroic beam-splitter BS1 and then sent via the galvanometer scanners SX and SY to the sample. BS1 is a hot mirror that reflects light of wavelengths longer than 1 μm . Two telescopes incorporated between these elements conveniently alter the diameter of the beam to match the aperture of different elements in the probing path and convey a probing beam of around 8 mm in diameter through the microscope objective (MO) pupil plane. The two transverse scanners SX and SY are separated here using telescopes to project a flat wavefront on the target under high NA. Lenses L1, L2, and L4 have focal lengths of 7.5 cm, while lens L3 has a focal length of 3 cm. The MO is a scan lens (focal length 1.8 cm) specially designed by ThorLabs to

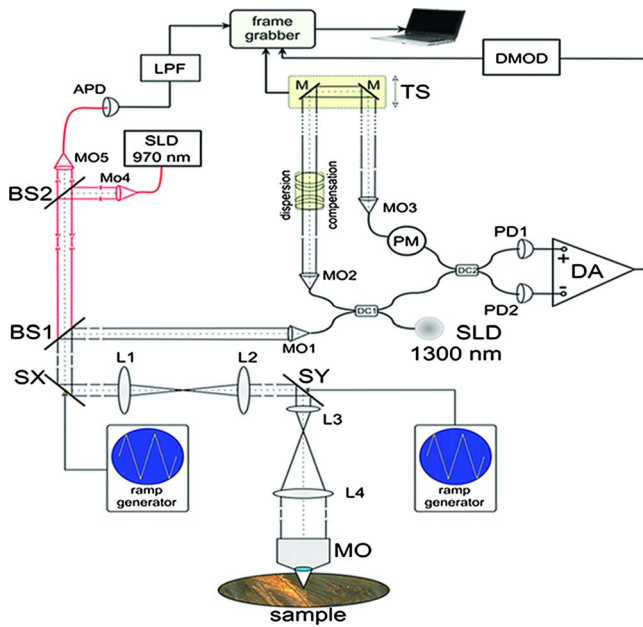


Fig. 1 *En-face* OCT at 1300 nm/confocal at 970 nm system. SLD = superluminescent diodes. SX, SY: X and Y scanners. APD: avalanche photodiode. L1, L2, L3, L4: lenses. MO1-5: microscope objectives. PD1, 2: pin photodetectors. BS1: dichroic beamsplitter. BS2: beam-splitter (20/80). LPF: low pass filter. PM: polarization controller. TS: translation stage.

prevent image degradation and distortion during scanning. Hence, a lateral resolution of around $2\ \mu\text{m}$ in the confocal channel and better than $5\ \mu\text{m}$ in the OCT channel is obtained. Light backscattered by the sample passes a second time through the object arm and is guided via the first directional coupler toward the second single mode directional coupler, where it interferes with that coming from the reference arm. Both output fibers from the second coupler are connected to two pin photodetectors, PD1 and PD2, in a balanced photo-detection unit constructed using a differential amplifier (DA). The OCT signal is rectified and low pass filtered in the demodulator (DMOD).

The confocal channel operates at a different wavelength than that of the OCT, to allow the utilization of a high gain silicon avalanche photodiode (APD). Light from a superluminescent diode at 970 nm is collimated by a microscope objective MO4 and reflected by a splitter BS2 (20% reflection) toward BS1. Light at 970 nm is transmitted via BS1 and BS2 toward the APD. The photodetected signal is amplified and low pass filtered in LPF. A computer-driven translation stage (TS) is used to alter the reference path length to acquire C-scan image frames from different depths and provide depth scanning in the B-scan regime.

The scanning procedure is similar to that used in any confocal microscope, where the fast scanning is *en face* (line rate, using the scanner SX) and the frame scanning is much slower (at the frame rate, using the scanner SY).²⁵ The frame grabber in Fig. 1 is controlled by signals from the generators driving the X scanner and the Y scanner. The SX galvanoscanner is driven with a ramp at 500 Hz and the SY galvanoscanner with a ramp at 2 Hz. In this way, an *en-face* image, in the plane (x, y) is generated at constant depth. The next *en-face* image

at a new depth is then generated by moving the translation stage (TS) in the reference arm of the interferometer and repeating the (x, y) scan. Ideally, the depth interval between successive frames should be much smaller than the system resolution in depth, and the depth change is applied only after the entire *en-face* image has been collected. However, in practice, to speed up the acquisition, the translation stage was moved continuously.

To construct B-scan images, no signal is applied to the frame scanner, the line scanner is driven with the same signal as in the C-scanning regime, and the translation stage (TS) is moved along the optical axis of the reference beam. In this case, the frame grabber is controlled by signals from the generator driving the SX-scanner (or the SY-scanner) with a ramp at 500 Hz, and TS is moved over the depth range required in 0.5 s. In this case, an OCT cross section image is produced either in the plane (x, z) or (y, z).

In the images presented next, no other phase modulation was employed apart from that introduced by the galvanometer scanner^{26,27} determining the line in the raster.

The other system contains an OCT channel only, employing a two coupler configuration similar to that in Fig. 1, with the difference that the X and Y scanners are grouped spatially. Only one lens of focal length 4 cm is used between the XY scanner head and the sample, allowing a larger lateral size image. Consequently, the transversal resolution is reduced to $15\ \mu\text{m}$. The X and Y scanners are similar and driven at the same line rate (500 Hz) and frame rate (2 Hz) as in the previous system.

Both systems can be sequentially switched between the *en-face* regime and the cross section regime. In this way, images with different orientations can be obtained using the same system.

2.5 Study Groups

In this study we investigated dental prostheses (group 1) and teeth with various treatment methods (group 2) used in dentistry.

Group 1 included several types of prostheses, such as: metal-ceramic fixed partial prostheses, metal-ceramic crowns, metal-polymer fixed partial prostheses, metal-polymer crowns, polymer and all-ceramic fixed partial prostheses, and complete dentures. The main goal in imaging this group was to detect the presence or absence of material defects and microleakage at the prosthetic interfaces.

Group 2 was composed from teeth with several treatment methods. For this group, the main goal was to investigate the quality of the endodontic treatment, enamel conditioning, and coronal filling. After extraction, the teeth were stored for no longer than 48 h in saline solution until sample preparation. The debris and calculus were removed using an ultrasonic scaler. Then, the teeth were carefully cleaned with pumice and rotary brushes. To avoid creating differences among the samples, the brushes were replaced after every fifth tooth. Then, the samples were used for cavity preparation, root canal treatment and filling, and for the subsequent application of orthodontic brackets, as follows.

- Class 5 cavities (cavities from the cervical area of the tooth) were prepared to assess the material defects and microleakage at the tooth-filling interfaces. Then the cavities

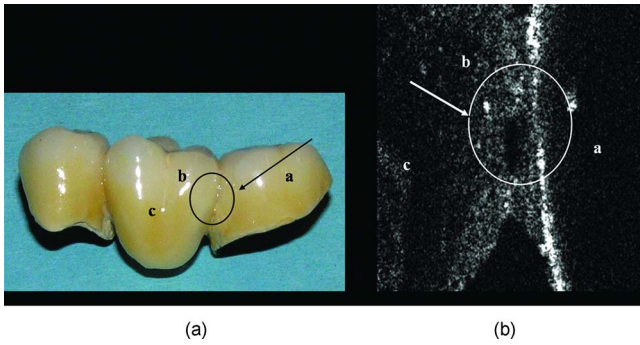


Fig. 2 (a) Metal-ceramic fixed partial prosthesis. (b) C-scan OCT image matching the depth of the defect at b approx 0.2 mm measured in air from the top, lateral size 9.5×9.5 mm. The image shows the interface between pillar crown (part a) and pontic (part c) in a metal-ceramic fixed partial prosthesis. The defect inside the ceramic layers is in the center of the circle at b.

were filled with composite resin. The composite restorations were finished and polished using a fine grit diamond bur and Kerr-Hawe polishing disks.

- Single rooted teeth only with one straight root canal were used for the assessment of the presence or absence of apical microleakage (gaps between the root canal wall, root canal sealer, and gutapercha cones). The root canals were prepared mechanically and filled with endodontic sealer and gutapercha cones.

- For the evaluation of the orthodontic attachment microleakage at the interfaces, the teeth were conditioned in order to receive orthodontic appliances.

3 Results

All depths in the C- and B-scan images presented next are measured in air, as determined by the axial translation of the translation stage. To infer the depth in the sample, the distance in air should be divided by its index of refraction. This varies depending on the material investigated; however, a rough approximation in the dental tissue⁶ can be obtained by dividing the distances quoted in air by 1.4.

3.1 Group 1

Material defects and aeric inclusions were identified as displayed in Figs. 2–4. In Fig. 5, the defect occurred due to the inadequate marginal adaptation of a metal-polymer crown to the supporting pillar.

Figure 2 refers to a case of a three unit metal-ceramic fixed partial prosthesis. OCT allows identification of a material defect inside the ceramic layers between the pillar crown and the pontic. The size of the defect is in the range of submillimeter and is wholly included in the ceramic. These particularities make such defects undetectable by any other noninvasive technique. The defect may lead to fracture of the ceramic component under usual masticatory forces.

Figure 3 shows a case of a metal-polymer fixed partial prosthesis with an aeric inclusion at the metal-polymer junction. We have noticed that, in general, defects in polymers were much larger than defects observed in ceramics. This is the case in Figs. 3(b) (C-scan) and 3(c) (B-scan), where the

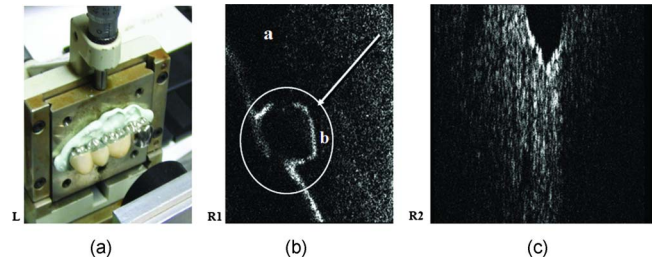


Fig. 3 (a) Metal-polymer fixed partial prosthesis in front of the scanning head. (b) C-scan OCT image. Part a shows approximately 0.5 mm depth measured in air from the top of the polymer; part b shows aeric inclusion at the metal-polymer junction. (c) B-scan OCT image that displays the cross section through the defect, with a depth of 1.8 mm measured in air along the vertical axis. 4×4 mm lateral size in both (b) and (c).

size is larger than 1.5 mm. The two images complement each other and provide more complete information than a single C-scan or B-scan image.

Since the surface of the sample will not generally be exactly perpendicular to the optical axis, B-scans will sometimes exhibit structure more commonly associated with C-scans and vice versa (effectively, there is a “tilt” in the image). Having access to both types of scans in realtime allows a clinician or dental technician to visualize such effects conveniently and without recourse to time-consuming 3-D reconstructions.

For a different metal-polymer crown, Fig. 5 shows C-scan images from an incorrect marginal fit of the crown on the abutment tooth, resulting in a space in the cervical area between the crown and the tooth with the luting cement, as indicated by part b. The image in Fig. 5 R presents a zoom into the area encircled in the bottom of Fig. 5(a).

Two esthetic fixed partial prostheses without metal frames are presented in Fig. 4. Voids are distinguished within the material volume; these are not detectable with any other known noninvasive technique. Their presence could lead to major fractures of prostheses, a problem analyzed in a recently published report.²⁸ Figures 4(a) and 4(b) refer to the

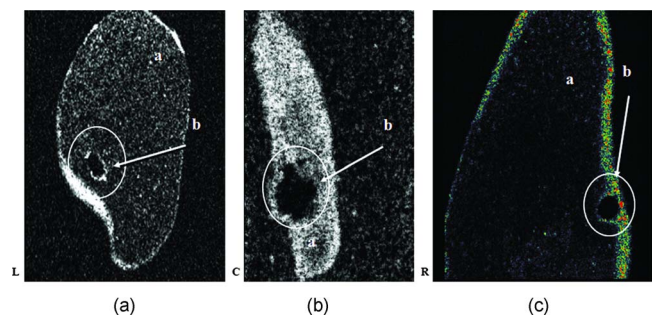


Fig. 4 C-scan OCT images from esthetic fixed partial prostheses. (a) and (b) refer to the same polymer prosthesis; images are acquired from different depths and with different lateral size. (a) $140 \mu\text{m}$ from the top measured in air, with a void well defined inside the material; (b) Zoom image (4×4 -mm lateral size) and deeper than in (a) by $100 \mu\text{m}$. (c) All ceramic crown (pressed ceramic technology). Part a: crown and part b: defect inside the ceramic layers at approximately $600 \mu\text{m}$ depth measured in air.

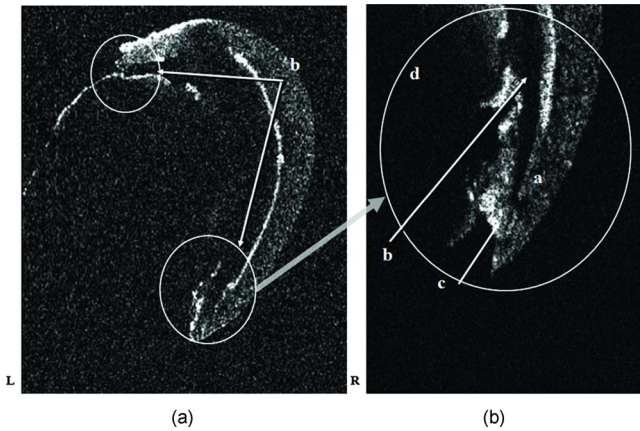


Fig. 5 C-scan images from a metal-polymer veneer crown at two magnifications, showing an incorrect marginal fit. Lateral size: (a) 9.5×9.5 mm; (b) 4×4 mm. The image in (b) is the magnification of the area in the bottom of the image (a). Part a shows the metal-polymer crown; part b the empty space between the crown and the pillar tooth; part c the luting cement; and part d the pillar tooth.

same polymer prosthesis, while Fig. 4(c) shows an *en-face* slice from an all-ceramic crown at proximal incidence. These esthetic restorations are more expensive than those with metal frames, and this reason alone enhances the need for a tool such as OCT to avoid the high repair costs incurred by patient and practitioner. In fact, these cannot be repaired and their replacement is the only solution.

3.2 Group 2

For the second group, teeth with several treatment methods are imaged to assess the material defects and microleakage at the tooth-filling interfaces, the presence or absence of apical microleakage and the quality of bracket bonding on dental hard tissue.

Figure 6(b) shows an *en-face* OCT image from a tooth with a class 5 cavity filled with diacrylic composite resin [Fig. 6(a)]. The main goals of testing such samples are to evaluate the structural integrity of the filling and the possible coronal

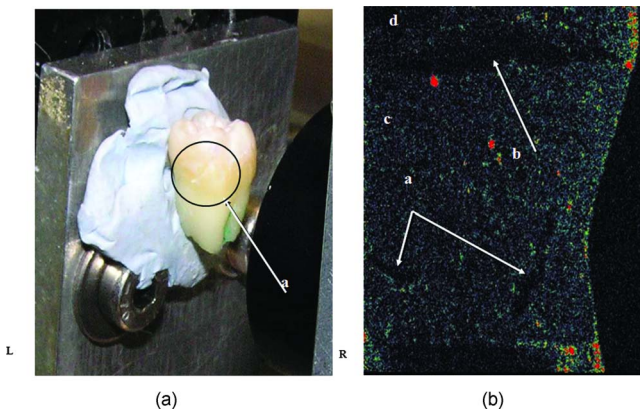


Fig. 6 (a) Tooth with a class 5 cavity filled with diacrylic composite resin in front of the OCT head. (b) 4×4 -mm lateral size, slice from a depth of $500 \mu\text{m}$ measured in air. Part a: gaps trapped inside the filling material; part b: coronal microleakage on the border of the resin filling; part c: composite resin filling; and part d: tooth.

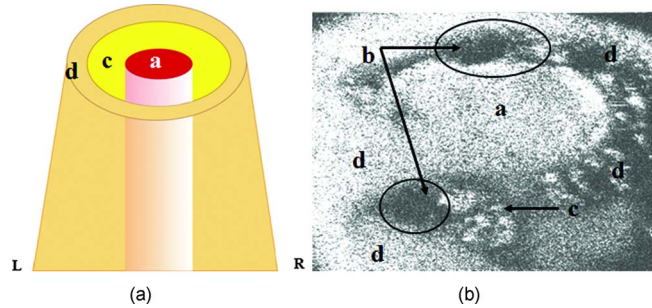


Fig. 7 (a) Schematic representation of tooth with the root canal filling (monoradicular tooth with endodontic treatment). (b) OCT C-scan image of root canal apical microleakage from a depth of $95 \mu\text{m}$ measured in air; lateral image size 4×4 mm. Part a: gutapercha cone; part b: microleakage space; part c: root canal sealer; and part d: root canal walls.

marginal microleakage. In some cases we found gaps inside the diacrylic composite resin and coronal marginal microleakage of various dimensions and located at different levels.

The quality of the endodontic treatment and root canal filling, represented schematically in Fig. 7(a) was assessed using both systems. Apical microleakage areas were detected between the gutapercha cones, root canal walls, and the sealing material [Fig. 7(b)].

For better assessment of the quality of the endodontic treatment, the second system was used, which provides dual imaging, OCT/CM, and magnified view. The confocal image aids guidance and allows focus adjustment to the OCT investigation. Figure 8(a) shows the sample in front of the microscope objective in Fig. 1. Pairs of *en-face* OCT/confocal images are shown in Figs. 8(b) and 8(c). 3-D reconstructions were performed using dedicated computer software, as shown in Fig. 9.

Orthodontic attachments bonding strength cannot be measured with OCT; however, by identifying and visualizing the voids in the composite, the quality of the restoration can be estimated. OCT investigation provides information on the microleakage of the bracket's bonding—several gaps are seen

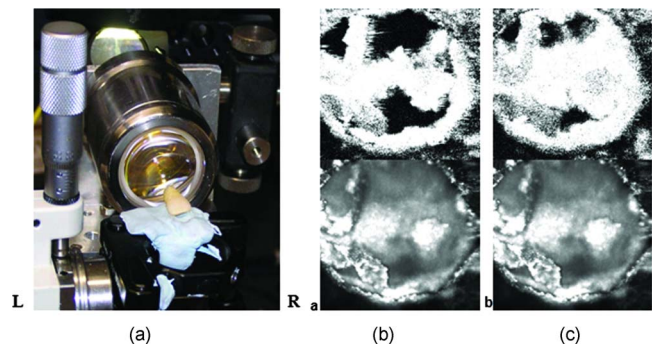


Fig. 8 Investigation of the same root canal filling in Fig. 7, using the second system (the dual *en-face* OCT/CM). (a) Photograph of tooth in front of the scanning head; (b) and (c) show pairs of confocal images (bottom) and *en-face* OCT images (top). In (c), the image in the OCT channel is deeper by $50 \mu\text{m}$ than in (b). Lateral image size in both the OCT and confocal images is 1×1 mm.

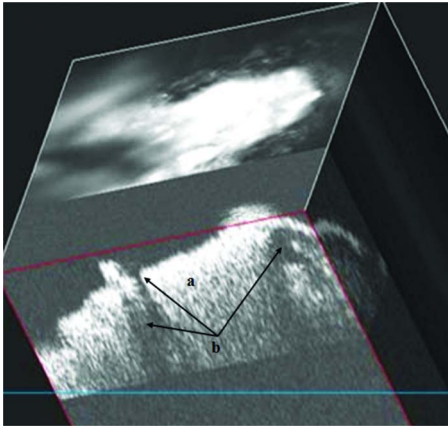


Fig. 9 3-D imaging of a root canal microleakage, inspected laterally, obtained from 39 pairs of OCT C-scan/CM images of 1×1 -mm lateral image size acquired at a $10\text{-}\mu\text{m}$ differential depth measured in air. Front: OCT image. Back: CM image. Part a: root canal sealer; and part b: microleakage space.

along the bracket base [Fig. 10(a)]. Also, a lack of adhesive material on the side of the bracket [Fig. 10(b)] is identified.

4 Discussions

OCT allows better characterization of dental prostheses. First, the detection of substance defects within the ceramic layers for metal-ceramic prostheses was demonstrated (Fig. 2). The detected defects have a large volume and therefore there is a high likelihood for fracture lines to be generated in the proximal area (Fig. 2). If the detection of such defects is feasible before inserting the prosthesis into the oral cavity, then timely corrective measures are possible to avoid the fracture of the ceramic component later on.

The images collected demonstrate that OCT can act as a valuable tool in imaging material defects in the metal-polymer fixed partial prostheses (Fig. 3). The volume gaps noted

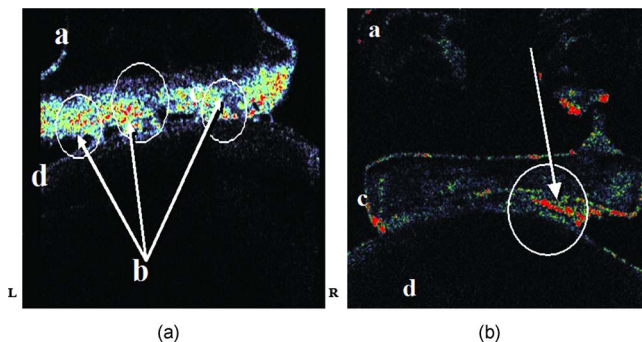


Fig. 10 (a) C-scan image of an adhesive bracket bonded on a vestibular maxillary premolar area. Part a: ceramic bracket; part b: gap trapped inside the adhesive resin between the bracket and the tooth; part c: adhesive resin layer; and part d: buccal area of the maxillary premolar. Depth measured in air: $60\ \mu\text{m}$. Lateral size: $4 \times 4\ \text{mm}$, (b) Adhesive bracket bonded on a vestibular maxillary premolar area. Part a: ceramic bracket; part b: lack of adhesive layer material in a large area between the bracket and the tooth; part c: adhesive resin layer; and part d: the vestibular area of the maxillary premolar. Depth from top, $160\ \mu\text{m}$ measured in air. Lateral size: $4 \times 4\ \text{mm}$.

within the polymers [Figs. 3(b) and 3(c), and Fig. 4(a)] are larger than those within the ceramics [Figs. 2(b) and 4(b)] which may possibly result in the fracture of the esthetic component of the prostheses. The repair procedures may lead often to the necessity of replacing the prostheses with new ones. Careful investigation of the metal-polymer prostheses accompanied by detection of the risk areas will allow corrective measures to reduce the likelihood of fractures of the polymer component.

Marginal adaptation of fixed partial prostheses still represents a challenge for both the dentist and technician. Generally, any technical laboratory is equipped with optical tools like microscopes that allow inspection of such areas. However, they cannot detect subtle structural effects due to stress. Therefore, there is a need for a better method to investigate the tooth-prosthesis interface. Ignoring this procedure may lead to the initiation of secondary caries of the abutments, washing of the luting cements, and major sensitivity of vital abutments to thermal and chemical stimuli. Such an investigation is hard to perform visually, mostly in the case of all-polymer or all-ceramic systems. It is practically impossible to investigate visually the cervical adaptation of the prostheses to the terminal area of the abutment. The OCT technique is suitable for the evaluation of the tooth-prosthesis interface before and after cementation (Fig. 5). In Fig. 5, the metal framework is well seen, as shown by the bright continuous border. Here the imaging proceeded *en face*, from cervical to the incisor (in opposition to Ref. 7), where the OCT image was perpendicular to the vestibular plane.

All ceramic restorations have recently entered the field of prosthodontics, offering improvements in esthetics. Early detection of substance defects within their layers [Fig. 4(c)] allows for optimal corrections before the restorations are inserted into the oral cavity. This will make their resistance to masticatory stress more reliable and will lead to a reduction in the number of fractures. For instance, Fig. 4(c) shows that the defect is situated in the superficial cervical area, in the maximum tension area recorded during mastication with high risks of fracture at this level.

For Group 2 samples, *en-face* OCT images have been generated from a depth of up to $1.5\ \text{mm}$. Cavities filled with composite resin have been imaged, showing voids within the restorative material. These may occur due to inadequate condensation. Also, gaps were visible at the tooth-restorative material interface, which are expected to reduce the time resistance of the filling and increase the risk of secondary caries occurrence. In Fig. 6, the interface between the dental structure and the filling composite resin is well distinguished. We can also make difference between the granular structure of the composite resin and the dental tissue (c and d within Fig. 6). Because the interface is well seen, we can also visualize any defects that might exit here or extend inside the material. In addition, in the inferior part of the composite filling (part c in Fig. 6), we can distinguish an interface with good contrast due to demineralization.¹¹ Thus, the OCT method presents potential for real time *in-vivo* investigation of the restorative treatments.

The apical filling of the root canal is considered to be the most microleakage-susceptible area of the root canal filling (Fig. 7). Figures 8 and 9 present dual *en-face* OCT/CM images of a root canal filling of a monoradicular tooth with

endodontic treatment. Gaps between the root canal walls and gutapercha cone on one hand and root canal walls and root canal sealer on the other hand are observed. To assess the root canal microleakage, it is necessary to understand the 3-D aspect of the root canal filling. Software visualization allows 3-D reconstruction of the apical area (Fig. 9). The 3-D software can be used for frontal, sagittal, and axial analysis of the samples.

For best stability of orthodontic appliances, ideally the resin shape should match the tooth shape. OCT can identify mismatches of the resin and the tooth shape. Voids may occur due to contraction caused by the curing process, or due to an inadequate application of the composite resin. OCT has the potential for both investigating the bracket bonding technique and for assessing the material defects inside the used composite resin. The images presented demonstrate the ability of the *en-face* OCT technique in detecting such voids [Figs. 10(a) and 10(b)]. Although this work refers to an *in-vitro* investigation, we believe that tooth-bracket interfaces could also be imaged *in vivo*.

5 Comments on the Technology

Currently, the most wide-spread OCT imaging technology is A-scan based. This has known significant advances recently due to the progress in spectral OCT, due to its better sensitivity²⁹ than its time domain counterpart, which allows faster data acquisition.

However, one of the main disadvantages of spectral OCT is the need to operate under fixed focus. This limits the imaging to low numerical aperture, which consequently determines low transversal resolution. A-scan-based OCT technology, such as spectral OCT, offers the user images with a single orientation in real time, B-scan. As another disadvantage, these cannot directly be put in correspondence with microscopy images (which have an *en-face* orientation).

The limitations of A- and B-scan OCT technology mentioned have led us to the construction of *en-face* OCT imaging systems. For applications such as that described here, time domain *en-face* OCT appears better suited for three reasons: 1. versatile orientation as mentioned; 2. focus control and dynamic focus, although not documented here, is currently implemented on system 2; and 3. an easier comparison with microscopy images.

The *en-face* OCT offers the user the possibility of rapidly acquiring sequential B- and C-scans by switching the instrument between the two regimes. The *en-face* scans provide an instant comparison to the familiar sight provided by direct view or by a conventional microscope. Features seen with the naked eye can easily be compared with features hidden in depth. Sequential and rapid switching between the *en-face* regime and the cross section regime, specific for the *en-face* OCT systems, represent a significant advantage in noninvasive imaging, as images with different orientations can be obtained using the same system.

This flexibility to obtain images in orthogonal planes in realtime is an advantage that is not present in even the fastest spectral systems.³⁰ The spectral OCT method, although generating faster B-scans than time domain OCT systems (such as the *en-face* OCT presented here), still requires significantly longer acquisition and processing time to generate a C-scan

image.³¹ This process requires the collection of the whole volume of the sample, processing the data to produce a 3-D volume, and then interpolation of the data volume to select a C-scan orientated cut. Even the fastest research systems require at least a second.³² To achieve 3-D reconstructions in a matter of seconds, transversal resolution is always compromised, which leads to lower transversal resolution in the *en-face* software reconstructed image.

In the current implementation, our frame rate is 2 Hz, i.e., a C-scan is produced in 0.5 s, in real time, which is less than any value reported by using spectral OCT to infer a C-scan by software means. In addition, by using resonant scanners³³ instead of the galvoscaners employed here, video rates become possible in *en-face* OCT as well. As a supplementary advantage, the transversal resolution is the same in both B- and C-scans. This is determined by the number of pixels in the T-scans, which are used to assemble B- and C-scans.

In our system, acquisition rates for both C and B-scans are the same, and the switching between one regime and the other requires the press of a keyboard key only.

6 Conclusions

The capability of *en-face* OCT imaging technology is assessed in: 1. providing early diagnosis of dental hard tissue, and 2. identifying material defects of dental prostheses and microleakages at prosthetic interfaces. Several types of dental treatments are evaluated, and the OCT imaging technique is applied to dental hard tissue, restorative materials, and to their interfaces and dental prostheses.

This is a preliminary *in vitro* study regarding the application of OCT in dentistry, generally and particularly in prosthodontics, conservative dentistry, endodontics, and orthodontics. Further *in-vivo* studies are necessary to extend the *en-face* OCT applications to other fields of dentistry, such as *in-vivo* imaging of hard and soft tissue.

We illustrate the applicability of the *en-face* OCT technology in imaging dental constructs, providing: 1. a differently oriented image than in the A-scan-based OCT reports; 2. choice of image orientation in rectangular planes; and 3. combination of the *en-face* OCT with confocal microscopy in one instrument for better guidance of the investigation.

Acknowledgments

This research was partially supported by several research grants of the Romanian National Authority for Scientific Research (CNCSIS At13/2005, CEEX 40/2006, CEEX 41/2006, CEEX 122/2006, CEEX 82/2006, CNCSIS A 1032/2007). The authors thank Ophthalmic Technologies Incorporated, Toronto, Canada, for the 3-D imaging program used in Fig. 9.

References

1. H. Y. Lin, B. Bowers, J. T. Wolan, Z. Cai, and J. D. Bumgardner, "Metallurgical, surface, and corrosion analysis of Ni-Cr dental casting alloys before and after porcelain firing," *Dent. Mater.* **24**, 378-385 (2008).
2. M. Rominu, S. Lakatos, Z. Florita, and M. Negrutiu, "Investigation of the mikroleakage at the interface between a Co-Cr based alloy and four polymer veneering materials," *J. Prosthet. Dent.* **87**, 620-624 (2002).
3. C. Sinescu, M. Negrutiu, D. Dodenciu, M. Rominu, and A. Stoaia, "Fixed partial dentures analysis using penetrating liquids. Comparative analysis with invasive methods (radiographic method)," *Timi-*

- soara Med. J.*, **56** (Suppl. 1), 73 (2006).
4. S. Lakatos, M. Rominu, M. Negrutiu, and Z. Florita, "The microleakage between alloy and polymer materials in veneer crowns," *Quintessence Int.* **34**, 295–300 (2003).
 5. D. Bratu and R. Nussbaum, "Bazele clinice și tehnice ale protezării fixe," *Editura Signata*, Timisoara, (in Romanian) (2001).
 6. F. Feldchtein, V. Gelikonov, R. Iksanov, G. Gelikonov, R. Kuranov, A. Sergeev, N. Gladkova, M. Ourutina, D. Reitze, and J. Warren, "In vivo OCT imaging of hard and soft tissue of the oral cavity," *Opt. Express* **3**, 239–250 (1998).
 7. L. L. Otis, M. J. Everett, U. S. Sathyam, and B. W. Colston Jr., "Optical coherence tomography: a new imaging technology for dentistry," *J. Am. Dent. Assoc.* **131**, 511–514 (2000).
 8. K. Nozaka, Y. Suruga, and E. Amari, "Microleakage of composite resins in cavities of upper primary molars," *Int. J. Paediatr. Dent.* **9**, 185–194 (1999).
 9. K. I. M. Delme, P. J. Deman, and R. J. G. De Moor, "Microleakage of class V resin composite restorations after conventional and Er:YAG laser preparation," *J. Oral Rehabil.* **32**, 676–685 (2005).
 10. L. S. A. De Melo, R. E. De Araujo, A. Z. Freitas, D. Zezell, N. D. Vieira Jr., J. Girkin, A. Hall, M. T. Carvalho, and A. S. L. Gomes, "Evaluation of enamel dental restoration interface by optical coherence tomography," *J. Biomed. Opt.* **10**, 064027 (2005).
 11. R. S. Jones, C. L. Darling, J. D. B. Featherstone, and D. Fried, "Remineralization of in vitro dental caries assessed with polarization-sensitive optical coherence tomography," *J. Biomed. Opt.* **11**, 014016 (2006).
 12. D. Fried, J. Xie, S. Shafi, J. D. B. Featherstone, T. M. Breunig, and C. Le, "Imaging caries lesions and lesion progression with polarization sensitive optical coherence tomography," *J. Biomed. Opt.* **7**(4), 618–627 (2002).
 13. R. S. Jones, M. Staninec, and D. Fried, "Imaging artificial caries under composite sealants and restorations," *J. Biomed. Opt.* **9**(6), 1297–1304 (2004).
 14. I. Miletic, G. Prpic-Mehific, T. Maruan, A. Tambie-Andrauevic, S. Pleuko, Z. Karlovic, and I. Anic, "Bacterial and fungal microleakage of AH26 and AH Plus root canal sealers," *Int. Endod. J.* **35**, 428–432 (2002).
 15. F. Dultra, J. M. Barroso, L. D. Carrasco, A. Capelli, D. M. Z. Guerisoli, and J. D. Pecora, "Evaluation of apical microleakage of teeth sealed with four different root canal sealers," *J. Appl. Oral Sci.* **14**, 341–345 (2006).
 16. H. Shemesh, G. van Soest, M. K. Wu, L. W. M. van der Sluis, and P. R. Wesselink, "The ability of optical coherence tomography to characterize the root canal walls," *J. Endod.* **33**, 1369–1373 (2007).
 17. C. C. Rosa, J. Rogers, J. Pedro, R. Rosen, and A. Podoleanu, "Multi-scan time domain OCT for retina imaging," *Appl. Opt.* **46**, 1795–1807 (2007).
 18. M. E. J. Van Velthoven, F. D. Verbraak, L. A. Yannuzzi, R. B. Rosen, A. G. Podoleanu, and M. D. De Smet, "Imaging the retina by *en-face* optical coherence tomography," *Retina J. Retinal Vitreous Diseases* **26**, 129–136 (2006).
 19. W. G. Chang, B. S. Slim, T. H. Yoon, Y. K. Lee, and C. W. Kim, "Effect of salicylic-lactic acid conditioner on the shear bond strength of brackets and enamel surfaces," *J. Oral Rehabil.* **32**, 287–295 (2005).
 20. A. G. Podoleanu and D. A. Jackson, "Combined optical coherence tomograph and scanning laser ophthalmoscope," *Electron. Lett.* **34**, 1088–1090 (1998).
 21. A. G. Podoleanu, G. M. Dobre, R. G. Cucu, and R. B. Rosen, "Sequential OCT and confocal imaging," *Opt. Lett.* **29**, 364–366 (2004).
 22. B. T. Amaechi, A. Podoleanu, S. M. Higham, and D. A. Jackson, "Correlation of quantitative light-induced fluorescence and optical coherence tomography applied for detection and quantification of early dental caries," *J. Biomed. Opt.* **8**(4), 642–647 (2003).
 23. J. A. Izatt, M. R. Hee, G. M. Owen, E. A. Swanson, and J. G. Fujimoto, "Optical coherence microscopy in scattering media," *Opt. Lett.* **19**, 590–593 (1994).
 24. A. G. Podoleanu, J. A. Rogers, D. A. Jackson, and S. Dunne, "Three dimensional OCT images from retina and skin," *Opt. Express* **7**, 292–298 (2000).
 25. B. R. Masters, "Three-dimensional confocal microscopy of the human optic nerve in vivo," *Opt. Express* **3**, 356–359 (1998).
 26. A. G. Podoleanu, G. M. Dobre, D. J. Webb, and D. A. Jackson, "Coherence imaging by use of a Newton rings sampling function," *Opt. Lett.* **21**, 1789–1791 (1996).
 27. A. Gh. Podoleanu, M. Seeger, G. M. Dobre, D. J. Webb, D. A. Jackson, and F. Fitzke, "Transversal and longitudinal images from the retina of the living eye using low coherence reflectometry," *J. Biomed. Opt.* **3**(1), 12–20 (1998).
 28. B. Taskonak, J. J. Mecholsky Jr., and K. J. Anusavice, "Fracture surface analysis of clinically failed fixed partial dentures," *J. Dent. Res.* **85**, 277–281 (2006).
 29. J. F. de Boer, B. Cense, B. H. Park, M. C. Pierce, G. J. Tearney, and B. E. Bouma, "Improved signal-tonoise ratio in spectral-domain compared with time-domain optical coherence tomography," *Opt. Lett.* **28**, 2067–2069 (2003).
 30. V. D. Madjarova, Y. Yasuno, S. Makita, Y. Hori, J. B. Voeffray, M. Itoh, and T. Yatagai "Investigations of soft and hard tissues in oral cavity by spectral domain optical coherence tomography," *Proc. SPIE* **6079**, 60790N (2006).
 31. A. G. Podoleanu, and R. B. Rosen, "Combinations of techniques in imaging the retina with high resolution," *Prog. Ret. Eye Res.* **27**(4), 464–499 (2008).
 32. R. Huber, D. C. Adler, V. G. Srinivasan, and J. G. Fujimoto, "Fourier domain mode locking at 1050 nm for ultra-high-speed optical coherence tomography of the human retina at 236,000 axial scans per second," *Opt. Lett.* **32**, 2049–2051 (2007).
 33. M. Pircher, B. Baumann, E. Gotzinger, and C. K. Hitzenberger, "Imaging the human retina and cone mosaic in vivo with PS-OCT," *Proc. SPIE* **6429**, 64290T (2007).